Synthesis, Characterization, and Luminescence Properties of the Ternary Europium Complex Covalently Bonded to Mesoporous SBA-15

Chunyun Peng,[†,‡] Hongjie Zhang,[*,†] Jiangbo Yu,[†] Qingguo Meng,[†] Lianshe Fu,[†] Huanrong Li,[†] Lining Sun,[†,‡] and Xianmin Guo[†,‡]

Key Laboratory of Rare Earth Chemistry and Physics, Changchun Institute of Applied Chemistry, Chinese Academy of Sciences, 5625 Renmin Street, Changchun 130022, People's Republic of China, and Graduate School of the Chinese Academy of Sciences, Beijing, People's Republic of China

Received: April 17, 2005; In Final Form: June 8, 2005

A novel mesoporous SBA-15 type of hybrid material (phen−SBA-15) covalently bonded with 1,10-phenanthroline (phen) ligand was synthesized by co-condensation of tetraethoxysilane (TEOS) and the chelate ligand 5-[*N*,*N*-bis-3-(triethoxysilyl)propyl]ureyl-1,10-phenanthroline (phen-Si) in the presence of Pluronic P123 surfactant as a template. The preservation of the chelate ligand structure during the hydrothermal synthesis and the surfactant extraction process was confirmed by Fourier transform infrared (FTIR) and ^{29}Si MAS NMR spectroscopies. SBA-15 consisting of the highly luminescent ternary complex Eu(TTA)$_3$phen (TTA = 2-thenoyltrifluoroacetone) covalently bonded to a silica-based network, which was designated as Eu(TTA)$_3$phen−SBA-15, was obtained by introducing the Eu(TTA)$_3$·2H$_2$O complex into the hybrid materials via a ligand exchange reaction. XRD, TEM, and N_2 adsorption measurements were employed to characterize the mesostructure of Eu(TTA)$_3$phen−SBA-15. For comparison, SBA-15 doped with Eu(TTA)$_3$·2H$_2$O and Eu(TTA)$_3$phen complexes and SBA-15 covalently bonded with a binary europium complex with phen ligand were also synthesized, and were named SBA-15/Eu(TTA)$_3$, SBA-15/Eu(TTA)$_3$phen, and Eu−phen−SBA-15, respectively. The detailed luminescence studies on all the materials showed that, compared with the doping sample SBA-15/Eu(TTA)$_3$phen and binary europium complex functionalized sample Eu−phen−SBA-15, the Eu(TTA)$_3$phen−SBA-15 mesoporous hybrid material exhibited higher luminescence intensity and emission quantum efficiency. Thermogravimetric analysis on Eu(TTA)$_3$phen−SBA-15 demonstrated that the thermal stability of the lanthanide complex was evidently improved as it was covalently bonded to the mesoporous SBA-15 matrix.

1. Introduction

Lanthanide complexes have long been known to give sharp, intense emission lines upon ultraviolet light irradiation, because of the effective intramolecular energy transfer from the coordinated ligands to the luminescent central lanthanide ion, which in turn undergoes the corresponding radiative emitting process (the so-called "antenna effect").[1] Therefore, they are expected to be promising luminescent dopants for the preparation of hybrid phosphors and other optical sources. In recent years, the luminescence properties of lanthanide complexes supported on a solid matrix have been studied extensively because their photophysical properties could be modified by interaction with the host structure.[2] For example, the incorporation of lanthanide complexes with β-diketones,[3] aromatic carboxylic acids,[4] and heterocyclic ligands[5] into sol−gel-derived host structures by covalent bonds has been extensively investigated. These studies indicate that the thermal stabilities and mechanical properties of the lanthanide complexes were improved by the matrixes.

Since their discovery in the early 1990s,[6] ordered mesoporous materials with unique properties (e.g., high surface area, high pore volume, controlled pore structure, and uniform pore size distribution) are of great interest for adsorption, sensing, catalysis, and other applications.[7] Recently, one of particular interest is the use of ordered mesoporous silica materials as a support for lanthanide complexes.[8] For example, Xu et al. reported that the lanthanide complex [$C_5H_5NC_{16}H_{33}$][Eu(TTA)$_4$] (TTA = 2-thenoyltrifluoroacetone) was incorporated into the surface-modified mesoporous molecular sieve Si-MCM-41 by the strong hydrogen bonding interactions between the rare-earth complex and the silylating agent.[8a,d] Meng et al. reported on the preparation of luminescent silica mesoporous molecular sieves MCM-48 activated by the europium complex Eu(DBM)$_3$·2H$_2$O (where DBM is dibenzoylmethane) by using a simple wet impregnation method.[8e] However, these investigations were mainly focused on doping mesoporous silica materials with lanthanide complexes, in which only weak physical interactions (hydrogen bonding, van der Waals force, or weak static effect) exist between the mesoporous silica materials and the lanthanide complexes. This will give little control over the clustering of emitting centers, inhomogeneous dispersion of both components, and leaching of the photoactive molecules in the obtained materials. Recently, our group has reported the synthesis of mesoporous silica MCM-41 covalently bonded with a binary europium complex with phen ligand (Eu−phen−MCM-41) via a co-condensation process.[9] This approach enables a higher and more homogeneous surface coverage of organosilane functionalities and can effectively prevent the aggregation of lanthanide

* To whom correspondence should be addressed. Fax: +86-431-5698041. E-mail: hongjie@ciac.jl.cn.

† Changchun Institute of Applied Chemistry, Chinese Academy of Sciences.

‡ Graduate School of the Chinese Academy of Sciences.

10.1021/jp051984n CCC: $30.25
Published on Web 07/23/2005

SCHEME 1: Synthesis Procedure and Predicted Structure of Eu(TTA)$_3$phen−SBA-15

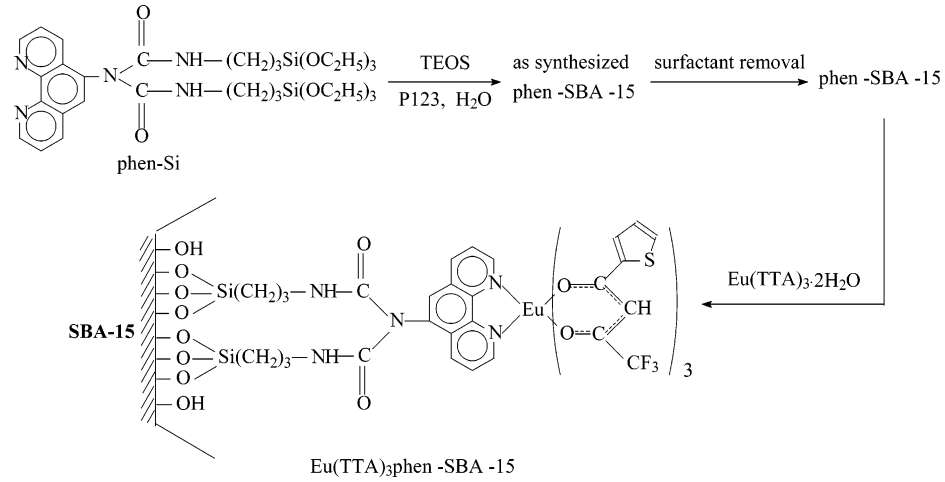

complexes. However, Eu−phen−MCM-41 shows relatively weak red luminescence and poor color purity because the water molecules in the first coordination sphere of europium(III) chloride phenanthroline complexes can deactivate the excited state of Eu^{3+} ion by means of energy transfer to the O−H vibration manifold. It is well-known that β-diketone ligand coordinating with the central Eu^{3+} ion can effectively prevent Eu^{3+} ion against the residual water molecules and silanol groups.[3,10] In the presence of β-diketone ligand, phen can successfully compete with the water molecules in the first coordination sphere around the Eu^{3+} ion. Moreover, as the first ligand, TTA transferred energy to Eu^{3+} ion more efficiently than phen ligand did.[11] Therefore, improved luminescence behavior can be expected via introduction of Eu(TTA)$_3$·2H$_2$O into the phen functionalized mesoporous silica matrix.

On the other hand, as a host material for lanthanide complexes, SBA-15 appears to be more attractive than mesoporous silicas M41S because of its much larger uniform pore size (up to 30 nm), thicker silica wall, and better stability.[12] For example, the larger pores make it an attractive host for the insertion of large amounts of bulky molecules with functional properties, and better stability makes it very suitable for immobilization of functional molecules. In particular, a few studies on the coordination of lanthanide ions or transition metal ions with organic ligands covalently bonded to SBA-15 mesoporous silica have been reported.[13] However, the synthesis and luminescence properties of SBA-15 mesoporous materials covalently bonded with organic lanthanide complexes have not been explored to date.

Herein, we report a direct synthesis of phen-functionalized SBA-15 mesoporous hybrid material (phen−SBA-15), in which phen was covalently bonded to the framework of SBA-15 by co-condensation of the modified phenanthroline 5-[*N*,*N*-bis-3-(triethoxysilyl)propyl]ureyl-1,10-phenanthroline (phen-Si) and tetraethoxysilane (TEOS) by using the Pluronic P123 surfactant as template. Highly luminescent complex Eu(TTA)$_3$phen-functionalized SBA-15 [denoted as Eu(TTA)$_3$phen−SBA-15] was obtained by introducing Eu(TTA)$_3$·2H$_2$O into the phen−SBA-15 hybrid materials with a ligand exchange reaction. Thus, the ternary europium complex Eu(TTA)$_3$phen was successfully linked to the framework of SBA-15 via a covalently bonded phen group. In addition, for comparison, SBA-15 doped with Eu(TTA)$_3$·2H$_2$O and Eu(TTA)$_3$phen complexes and SBA-15 covalently bonded with a binary europium complex with phen ligand were also synthesized, and are designated SBA-15/Eu-(TTA)$_3$, SBA-15/Eu(TTA)$_3$phen, and Eu−phen−SBA-15, respectively. Detailed analyses of luminescent properties of all these synthesized materials and the thermal stability of the resulting Eu(TTA)$_3$phen−SBA-15 were investigated in relation to guest−host interactions between the organic complex and the silica matrix.

2. Experimental Section

2.1. Materials. Tetraethoxysilane (TEOS, Aldrich), 3-(triethoxysilyl)propyl isocyanate (Aldrich), Pluronic P123 (Aldrich), and ethanol were used as received. The solvent chloroform ($CHCl_3$) was used after desiccation with anhydrous calcium chloride. Europium chloride ($EuCl_3$) and gadolinium chloride ($GdCl_3$) were obtained by dissolving Eu_2O_3 (99.99%, Shanghai Yuelong) and Gd_2O_3 (99.99%, Shanghai Yuelong) in hydrochloric acid, respectively.

2.2. Synthesis. *2.2.1. Synthesis of Phen-Functionalized SBA-15 Mesoporous Silica (phen−SBA-15).* The starting reagent 5-amino-1,10-phenanthroline (denoted as phen-NH$_2$) was prepared by the method of ref 14. Phen-Si was synthesized by the reaction of phen-NH$_2$ and 3-(triethoxysilyl)propyl isocyanate in $CHCl_3$ as described in ref 5a. Then 2.0 g of P123 was dissolved in 15 g of deionized water and 60 g of a 2 M HCl solution at 35 °C. A mixture of TEOS and phen-Si was added to that solution, leading to a composition with a molar ratio of *X* phen-Si:(1 − *X*) TEOS:0.0172 P123:6 HCl:208.33 H$_2$O, where $X = 0$, 0.02, 0.04, and 0.06. The mixture was stirred at 35 °C for 24 h and transferred into a Teflon bottle sealed in an antoclave, which was then heated to 100 °C for 2 days. The solid product was recovered by filtration, washed thoroughly with deionized water, and air-dried at room temperature. Removal of copolymer surfactant P123 was conducted by Soxhlet extration with ethanol for 24 h to give the sample denoted as phen−SBA-15(*X*) ($X = 0$, 0.02, 0.04, and 0.06), where *X* is the phen-Si:(TEOS + phen-Si) molar ratio.

2.2.2. Synthesis of SBA-15 Mesoporous Silica Covalently Bonded with Ternary Complex Eu(TTA)$_3$Phen [Eu(TTA)$_3$phen−SBA-15]. Eu(TTA)$_3$·2H$_2$O was prepared by the methods described in the literature.[15] While being stirred, phen−SBA-15(0.04) was soaked in an excess of an Eu(TTA)$_3$·2H$_2$O ethanol solution [2 equiv of Eu(TTA)$_3$·2H$_2$O per phen moiety]. The mixture was heated under reflux for 12 h, followed by filtration and extensive washing with acetone for removal of the excess of Eu(TTA)$_3$·2H$_2$O. The resulting Eu(TTA)$_3$phen−SBA-15 was dried at 60 °C under vacuum overnight. The hybrid mesoporous product Eu(TTA)$_3$phen−SBA-15 was obtained as outlined in Scheme 1.

2.2.3. Synthesis of SBA-15 Covalently Bonded with the Europium Complex with Phen Ligand (Eu−phen−SBA-15). The synthesis procedure for Eu−phen−SBA-15 was similar to that of $Eu(TTA)_3$phen−SBA-15 except that $Eu(TTA)_3{\cdot}2H_2O$ was replaced by $EuCl_3$.

2.2.4. Synthesis of SBA-15 Doped with the $Eu(TTA)_3{\cdot}2H_2O$ Complex [SBA-15/$Eu(TTA)_3$]. SBA-15 doped with $Eu(TTA)_3{\cdot}2H_2O$ [SBA-15/$Eu(TTA)_3$] was prepared in the same way as described for $Eu(TTA)_3$phen−SBA-15 except that phen−SBA-15 was replaced by pure SBA-15.

2.2.5. Synthesis of SBA-15 Doped with the $Eu(TTA)_3$Phen Complex [SBA-15/$Eu(TTA)_3$phen]. The $Eu(TTA)_3$phen complex was synthesized following the literature procedure.[16] The synthesis procedure for SBA-15/$Eu(TTA)_3$phen was also similar to that of $Eu(TTA)_3$phen−SBA-15 except that phen−SBA-15 and $Eu(TTA)_3{\cdot}2H_2O$ were replaced by pure SBA-15 and the $Eu(TTA)_3$phen complex, respectively.

2.2.6. Synthesis of the $Gd(Phen)_3Cl_2$ Complex. At room temperature, 3 mmol of phen was dissolved in 10 mL of ethanol. Then 1 mmol of a $GdCl_3$ ethanol solution was added under stirring, and the solution was heated under reflux for 2 h. The white powder was filtered and washed with ethanol. The resulting $Gd(phen)_3Cl_2$ was dried at 60 °C under vacuum overnight.

2.3. Characterization. Small-angle X-ray diffraction patterns (XRD) were recorded with Rigaku-Dmax 2500 diffractometer using Cu Kα radiation (40 kV and 200 mA) at a step width of 0.02°. Fourier transform infrared (FTIR) spectra were measured within the 4000−400 cm^{-1} wavenumber range using a Perkin-Elmer model 580B IR spectrophotometer with the KBr pellet technique. Solid-state ^{29}Si MAS NMR spectra were recorded at 79.46 MHz, using a Bruker Avance 400 spectrometer. The mesostructure of the $Eu(TTA)_3$phen−SBA-15 hybrid material was proven with a transmission electron microscope (TEM, JEM-100CX(II)). Nitrogen (N_2) adsorption/desorption isotherms were measured by using a Nova l000 analyzer with nitrogen. The samples were outgassed for 4 h at 120 °C before the measurements. Surface areas were calculated by the Brunauer−Emmett−Teller (BET) method and pore sizes by the Barrett−Joyner−Halenda (BJH) methods. The content of Eu^{3+} ion was obtained by inductively coupled plasma-atomic emission spectroscopy and mass spectroscopy (ICP-AES−MS) with a TJA-POEMS spectrometer. The UV−vis absorption spectra were recorded with a TU-1901 spectrophotometer. The fluorescence excitation and emission spectra were obtained with a Hitachi F-4500 spectrophotometer equipped with a 150 W xenon lamp as the excitation source. Luminescence lifetimes were measured with a Lecroy Wave Runner 6100 digital oscilloscope (1 GHz) using different wavenumber lasers (pulse width of 4 ns) as the excitation source (Continuum Sunlite OPO). All the measurements were performed at room temperature. The low-temperature phosphorescence spectrum of the Gd^{3+} complex was measured on a Hitachi F-4500 spectrophotometer at liquid nitrogen temperature (77 K). Thermogravimetric analysis (TGA) was performed on a Perkin-Elmer Pyris Diamond thermal analyzer up to 700 °C at a heating rate of 10 °C/min under N_2.

3. Results and Discussion

3.1. Phen-Functionalized Mesoporous Silica SBA-15. Mesoporous silica containing phen groups was synthesized as described in the Experimental Section. During the synthesis, a series of phen-functionalized SBA-15 samples with different concentrations of phen-Si in the initial mixture were obtained. Figure 1 depicts the variation of the XRD patterns for the resulting phen−SBA-15(X) (X = 0, 0.02, 0.04, and 0.06). For the samples synthesized with phen-Si:(phen-Si + TEOS) molar ratios below 0.04, three well-resolved diffraction peaks [(100), (110), and (200) reflections] in the 2θ range of 0.8−2°, typical of hexagonal SBA-15, are observed. However, with the concentration of phen-Si increasing, the intensity of the (100) reflection decreases gradually and the higher-angle peak (110) and (200) reflections diminish in relative intensity [disappearing entirely for phen−SBA-15 (0.06)]. The reduction in diffraction intensity with an increase in phen-Si concentration can be partly assigned to a decrease in the mesoscopic order of the materials, such as variations in the wall thickness, and may also be partly due to the contrast matching between the amorphous silicate framework and organic moieties inside the pore channels of the materials.[17] The results described above show that the formation and self-assembly of surfactants aggregates might be perturbed during the co-condensation when the phen-Si:(phen-Si + TEOS) molar ratio is ≥0.06, and an optimum molar ratio [phen-Si:(phen-Si + TEOS) = 0.04] can be employed to synthesize phen-functionalized SBA-15 with a high loading of functionality yet a good mesostructure. Hence phen−SBA-15-(0.04) was selected as the candidate for the following preparation of SBA-15 mesoporous silica covalently bonded with the Eu-$(TTA)_3$phen complex [$Eu(TTA)_3$phen−SBA-15].

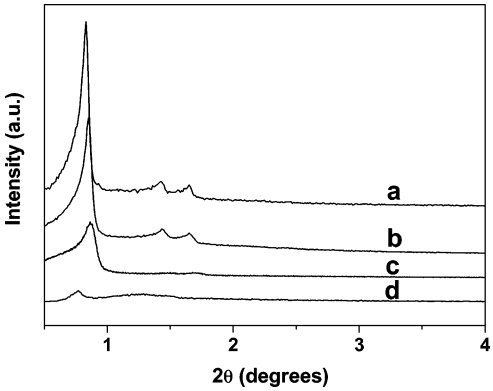

Figure 1. XRD patterns of phen−SBA-15(X), when X = (a) 0, (b) 0.02, (c) 0.04, and (d) 0.06.

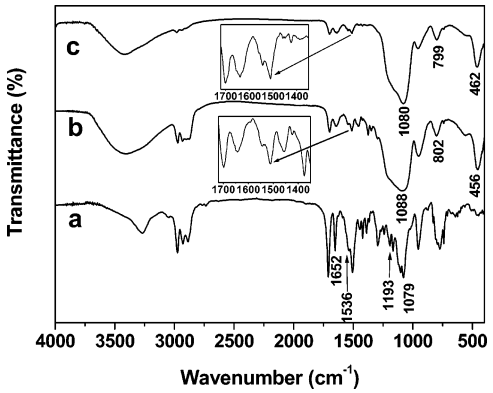

Figure 2. FTIR spectra for phen-Si (a), as-synthesized phen−SBA-15(0.04) (b), and surfactant-extracted phen−SBA-15(0.04) (c).

The presence of the organic ligand covalently bonded to the mesoporous SBA-15 was characterized by FTIR and ^{29}Si MAS NMR spectroscopy. The FTIR spectra of phen-Si (a), as-synthesized phen−SBA-15(0.04) (b), and surfactant-extracted phen−SBA-15(0.04) (c) are shown in Figure 2. In Figure 2a, the spectrum of phen-Si is dominated by ν(C−Si,1193 cm^{-1}) and ν(Si−O,1079 cm^{-1}) absorption bands, characteristic of trialkoxylsilyl functions. In panels b and c of Figure 2, the

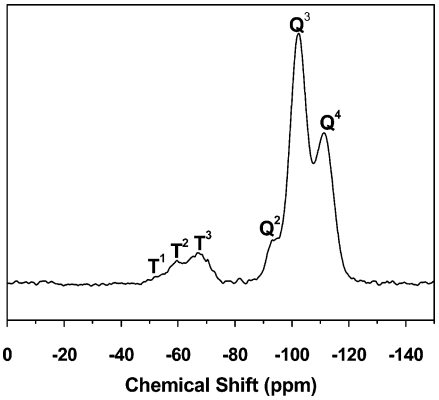

Figure 3. ^{29}Si MAS NMR spectrum of the phen−SBA-15(0.04).

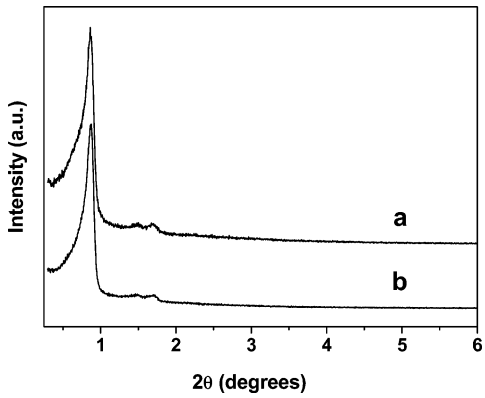

Figure 4. XRD patterns of phen−SBA-15(0.04) (a) and Eu(TTA)$_3$phen−SBA-15 (b).

formation of the Si−O−Si framework is evidenced by the bands located at 1088 and 1080 cm^{-1} (ν_{as}, Si−O), 802 and 799 cm^{-1} (ν_s, Si−O), and 456 and 462 cm^{-1} (δ, Si−O−Si) (ν represents stretching, δ in-plane bending, s symmetric, and as asymmetric vibrations). The peaks at 1652 and 1536 cm^{-1}, originating from the CONH group of phen-Si, can also be observed both in the as-synthesized material and in the surfactant-extracted material, which is consistent with the fact that the phen group in the framework remains intact after both the hydrolysis−condensation reaction and the surfactant extraction procedure. In addition, the surfactant-extracted phen−SBA-15 only exhibits weak templete ν(C−H) vibrations at 2700−3000 cm^{-1} and a disappearance of δ_s(C−H) vibrations at 1375 cm^{-1}, which confirms that most of the surfactant has been removed.

^{29}Si MAS NMR spectroscopy results of the surfactant-extracted phen−SBA-15(0.04) mesoporous silica sample are displayed in Figure 3. The peaks corresponding to the various siloxane Q^m [$Q^m = Si(OSi)_m(OH)_{4-m}$, $m = 2-4$] and organosiloxane T^n [$T^n = RSi(OSi)_nOH_{3-n}$, $n = 1-3$] species can be identified clearly. The relative integrated intensities of the organosiloxane T^1, T^2, and T^3 NMR signals can be employed to estimate the degree of hydrolysis−condensation of organic functional groups. Compared with T^1 and T^2 organosiloxane centers, the predominance of T^3 [the T^3:($T^3 + T^2 + T^1$) ratio is 0.65] suggests that the hydrolysis and condensation of the organo functionality (phen-Si) in the order structure is nearly complete, indicating a strong linkage (three Si−O−Si covalent bonds) between the organic ligand and the silica matrix.

3.2. Ternary Complex of Eu(TTA)$_3$phen-Functionalized Mesoporous Silica SBA-15. The power X-ray diffraction analyses performed on phen−SBA-15(0.04) (a) and Eu(TTA)$_3$phen−SBA-15 (b) are compared in Figure 4. These patterns feature distinct Bragg peaks in the 2θ range of 0.8−2°, which can be indexed as (100), (110), and (200) reflections of a two-dimensional hexagonal (*p*6*mm*) structure of SBA-15 material. The values of the corresponding unit cell parameter *a* ($a = 2d_{100}/\sqrt{3}$) of phen−SBA-15(0.04) and Eu(TTA)$_3$phen−SBA-15 are 11.74 and 11.69 nm, respectively. Compared with that of phen−SBA-15(0.04), the d_{100} spacing value of Eu(TTA)$_3$phen−SBA-15 is nearly unchanged, indicating that the framework hexagonal ordering has been retained very well upon the introduction of Eu(TTA)$_3$·2H$_2$O. The diffraction pattern of phen−SBA-15(0.04) exhibits an intensity greater than that of Eu(TTA)$_3$phen−SBA-15. The reduction in diffraction intensity upon the introduction of Eu(TTA)$_3$·2H$_2$O into phen−SBA-15 may be assigned to the presence of Eu(TTA)$_3$phen inside the pore channels of Eu(TTA)$_3$phen−SBA-15.

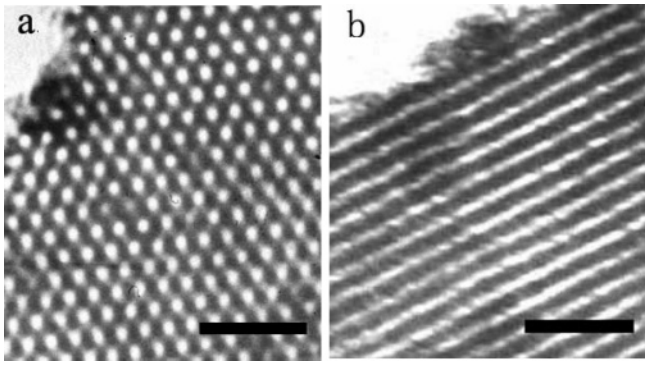

Figure 5. TEM images of Eu(TTA)$_3$phen−SBA-15 recorded along the [100] (a) and [110] (b) zone axes. Both scale bars are 50 nm.

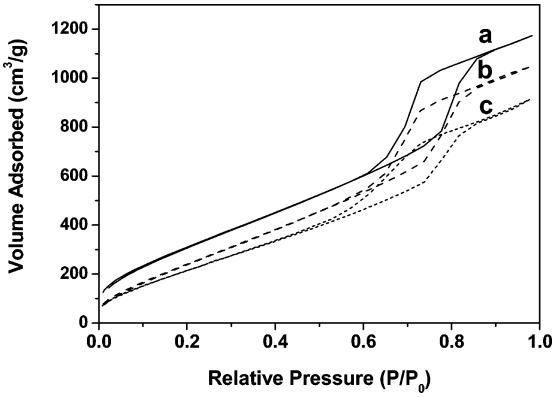

Figure 6. N_2 adsorption and desorption isotherms of SBA-15 (a, —), phen−SBA-15(0.04) (b, − − −), and Eu(TTA)$_3$phen−SBA-15 (c, - - -).

The hexagonal symmetry of Eu(TTA)$_3$phen−SBA-15 inferred from XRD is also in agreement with the TEM investigation. TEM images of Eu(TTA)$_3$phen−SBA-15 are presented in Figure 5 and confirm the suggested *p*6*mm* symmetry, indicating that after the complexation process the mesostructure of the Eu(TTA)$_3$phen−SBA-15 sample can be substantially conserved. The distance between the centers of the mesopores is estimated to be 11 nm, in good agreement with the value determined from the corresponding XRD data.

The N_2 adsorption/desorption isotherms of phen−SBA-15-(0.04), Eu(TTA)$_3$phen−SBA-15, and pure SBA-15 samples are shown in Figure 6. The textural data of the materials are given in Table 1. All these samples display type IV isotherm curves with an H1 hysteresis at high relative pressure, characteristic of highly ordered mesoporous materials according to the IUPAC classification.[18] It can be seen that capillary condensation of N_2 occurred over slightly wider P/P_0 ranges in phen−SBA-15-

TABLE 1: Textural Data of SBA-15, Phen−SBA-15, and Eu(TTA)$_3$phen−SBA-15[a]

sample	d_{100} (nm)	a_0 (nm)	S_{BET} (m^2/g)	V (cm^3/g)	D (nm)	t (nm)
SBA-15	10.76	12.42	1197	1.81	7.39	5.03
phen−SBA-15	10.17	11.74	996	1.62	6.43	5.31
Eu(TTA)$_3$phen−SBA-15	10.12	11.69	872	1.41	5.77	5.92

[a] d_{100} is the $d(100)$ spacing, a_0 the cell parameter ($a_0 = 2d_{100}/\sqrt{3}$), S_{BET} the BET surface area, V the pore volume, D the pore diameter, and t the wall thickness, calculated by $a_0 - D$.

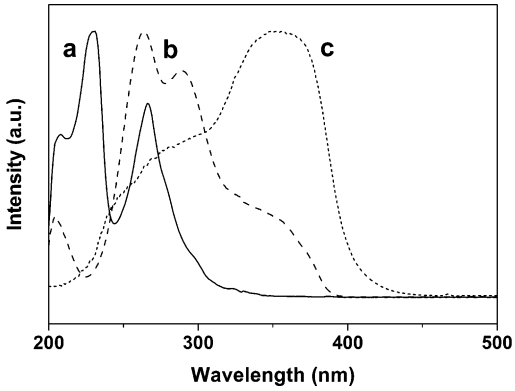

Figure 7. Absorption spectra of phen−Si (a, —) and TTA (b, − − −) at 1×10^{-4} mM in ethanol. The excitation spectrum for Eu(TTA)$_3$phen−SBA-15 as a solid (c, - - -) was monitored at 612 nm. All spectra are normalized to a constant intensity at the maximum.

(0.04) and Eu(TTA)$_3$phen−SBA-15 than in the pure SBA-15 sample. Phen−SBA-15(0.04) exhibits a smaller specific area and a slightly smaller pore size and pore volume in comparison with those of pure SBA-15, which might be due to the presence of both organic ligand phen on the pore surface and the co-surfactant effect of phen-Si, which interacts with surfactant and reduces the diameter of the micelles.[19] In addition, upon introduction of Eu(TTA)$_3$·2H$_2$O into the phen−SBA-15, the specific area, pore size, and pore volume of Eu(TTA)$_3$phen−SBA-15 are smaller than those of phen−SBA-15. This also confirmed the incorporation of the Eu(TTA)$_3$phen complex in the channels of SBA-15.

3.3. Luminescence Properties. *3.3.1. Antenna Effects and Luminescence*. The excitation spectrum of the resulting Eu(TTA)$_3$phen−SBA-15 and the absorption spectra of the ligands (TTA and phen-Si) are shown in Figure 7. The overlaps between the excitation band of Eu(TTA)$_3$phen−SBA-15 (Figure 7c) and the absorption bands that came from ligands TTA (Figure 7b) and phen-Si (Figure 7a) can be observed clearly, which indicates that the central Eu^{3+} ion in Eu(TTA)$_3$phen−SBA-15 can be efficiently sensitized by the ligands (TTA and phen), an antenna effect, and thus suggests that Eu^{3+} ion is surrounded by TTA and phen-Si.[20] In addition, the Förster model,[20a,21] which considers the overlap between the emission spectrum of the donor and the absorption spectrum of the acceptor, is essential for energy transfer phenomena. As Figure 8 demonstrates, the observed overlaps between the absorption spectrum of $EuCl_3$ in ethanol and the emission spectra of TTA and phen−SBA-15 lead to the conclusion that both the phen group covalently bonded to the SBA-15 and the ligand TTA can sensitize the luminescence of the central Eu^{3+} ion. Meanwhile, we observed that the overlap between the absorption band of ligand TTA and the excitation band is larger than that between the absorption band of ligand phen-Si and the excitation band, suggesting that TTA is a more efficient sensitizer than phen for the luminescence of the central Eu^{3+} ion and the intramolecular energy

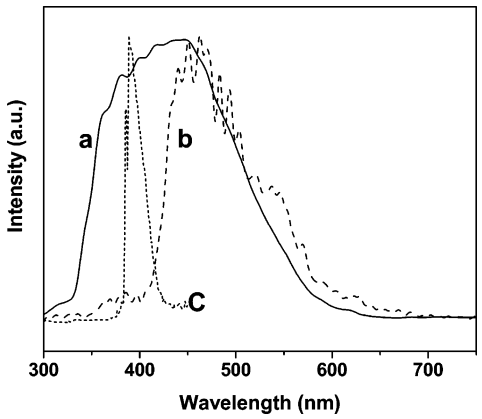

Figure 8. Emission spectrum of phen−SBA-15(0.04) (a, excited at 279 nm, —) and TTA (b, excited at 219 nm, − − −) as solids and absorption spectrum of $EuCl_3$ at 1×10^{-4} mM in ethanol (c, - - -). All spectra are normalized to a constant intensity at the maximum.

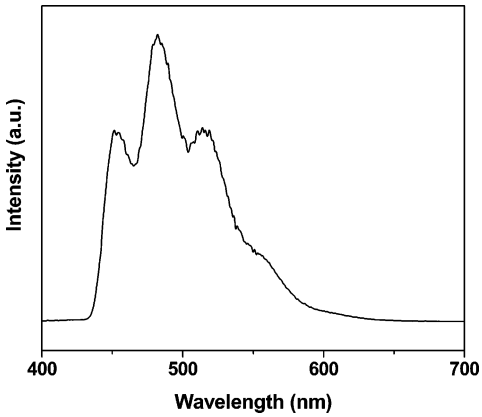

Figure 9. Emissiom spectrum of Gd(phen)$_3$Cl$_2$ at 77 K ($\lambda_{ex} = 298$ nm) at 5×10^{-4} M in methanol.

transfer in Eu(TTA)$_3$phen−SBA-15 occurs mainly between ligand TTA and the central Eu^{3+} ion.

The efficient ligand-to-metal ion energy transfers in Eu(TTA)$_3$phen−SBA-15 are also investigated by energy difference between the triplet states of ligands and the resonance energy level of the central lanthanide ion. The efficiency of the intramolecular energy transfer was very sensitive to the energy levels of the triplet state of the ligand. According to the luminescence theory of lanthanide complexes,[1,22] the requirement for an efficient intramolecular energy transfer is that the energy difference between the triplet state of the ligand and the resonance energy level of the central Eu^{3+} ion be in the range of 500−2500 cm^{-1}. The triplet-state energy level of phen ligand is determined from the phosphorescence spectrum of the respective Gd^{3+} complex at 77 K under UV excitation.[1,22,23] Three phosphorescence bands are observed in the emission spectrum of Gd(phen)$_3$Cl$_2$ (Figure 9, excited at 298 nm). The triplet-state energy level of phen ligand was determined from the shortest-wavelength phosphorescence band (22 173 cm^{-1}) due to the 0−0 transition of phen ligand. It has been reported that the triplet-state energy level of TTA ligand[22c] is 20 400 cm^{-1} and the resonance energy level of Eu^{3+} ion[22a] is 19 020 cm^{-1}. Therefore, the energy differences between the triplet-state energy levels of TTA and phen ligands and the $^5D_1$ level of Eu^{3+} ion are 1380 and 3153 cm^{-1}, respectively. According to the luminescence theory of lanthanide complexes, the ligand TTA can sensitize Eu^{3+} ion luminescence efficiently and the

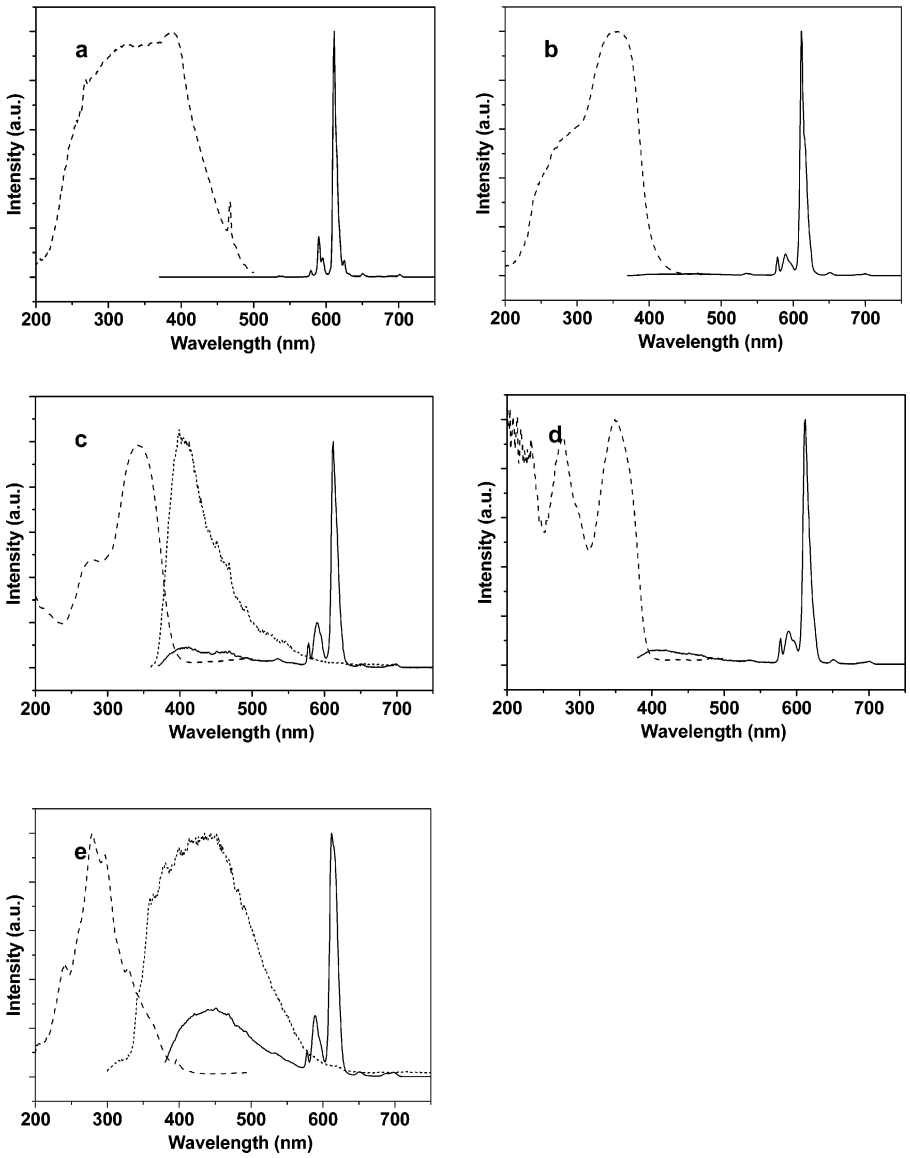

Figure 10. Excitation (− − −) and emission (—) spectra of Eu(TTA)$_3$phen (a, λ_{ex} = 385 nm), Eu(TTA)$_3$phen−SBA-15 (b, λ_{ex} = 352 nm), SBA-15/Eu(TTA)$_3$ (c, λ_{ex} = 341 nm) (- - -, the emission spectrum of SBA-15 excited at 350 nm), SBA-15/Eu(TTA)$_3$phen (d, λ_{ex} = 350 nm), and Eu−phen−SBA-15 (e, λ_{ex} = 279 nm) [- - -, the emission spectrum of phen−SBA-15(0.04) excited at 279 nm] as solids. All the excitation spectra were obtained by monitoring the emission wavelength of the Eu^{3+} ions at 612 nm. All spectra are normalized to a constant intensity at the maximum.

intramolecular energy transfer between TTA ligand and Eu^{3+} ion is more efficient than that between phen ligand and Eu^{3+} ion.

Figure 10 presents the normalized excitation and emission spectra for the Eu(TTA)$_3$phen complex (a), Eu(TTA)$_3$phen−SBA-15 (b), SBA-15/Eu(TTA)$_3$ (c), SBA-15/Eu(TTA)$_3$phen (d), and Eu−phen−SBA-15 (e) as solids at room temperature. The excitation spectra of the materials were obtained by monitoring the emission wavelength of the Eu^{3+} ions at 612 nm. As shown in Figure 10a, the excitation spectrum of the pure Eu(TTA)$_3$phen complex exhibits a broad excitation band (BEB) between 200 and 500 nm (λ_{max} = 385 nm), which can be assigned to the $\pi-\pi^*$ electron transition of the ligands.[11,24] A peak at 467 nm is observed due to the $f-f$ absorption transition ($^7F_0 \rightarrow {}^5D_2$) of Eu^{3+} ion. This transition is weaker than the absorption of the organic ligands and overlapped by BEB, which proves that luminescence sensitization via excitation of the ligands is much more efficient than the direct excitation of the Eu^{3+} ion absorption level. As no emission from the ligands is detected, the emission spectrum (excited at 385 nm) displays only the intra-4f^6 $^5D_0 \rightarrow {}^7F_J$ (J = 0, 1, 2, 3, or 4) transitions of Eu^{3+} ion; this energy transfer process seems to be very efficient for the Eu(TTA)$_3$phen complex. The observed number of Stark components for $^5D_0 \rightarrow {}^7F_J$ (J = 0, 1, and 2) transitions is 1, 3, and 5, respectively. The other transitions are negligible since their intensities are weak and their Stark components are not completely resolved. The stark splitting reveals an ordered "crystalline" rare-earth ion environment, rather than an amorphous one.[8b] However, for Eu(TTA)$_3$phen−SBA-15 (Figure 10b), the excitation spectrum become narrower than that of the Eu(TTA)$_3$phen complex and the maximum excitation shifted from 385 to 352 nm. This pronounced blue shift of the excitation band as the introduction of the europium complex into the SBA-15 was attributed to a hypsochromic effect resulting from the change in the polarity of the environment surrounding the europium complex in the mesoporous silicas SBA-15.[8e] No $f-f$ transition of Eu^{3+} ion could be observed in the spectrum, indicating that the energy transfer from the ligands to Eu^{3+} ion is more efficient in Eu(TTA)$_3$phen−SBA-15 than in the pure Eu(TTA)$_3$phen complex. Excitation at 352 nm provides the

TABLE 2: Photoluminescent Data of Eu(TTA)$_3$phen, Eu(TTA)$_3$phen−SBA-15, SBA-15/Eu(TTA)$_3$, SBA-15/Eu(TTA)$_3$phen, and Eu−phen−SBA-15 as Solids[a]

	Eu(TTA)$_3$phen	Eu(TTA)$_3$phen−SBA-15	SBA-15/Eu(TTA)$_3$	SBA-15/Eu(TTA)$_3$phen	Eu−phen−SBA-15
ν_{00} (cm^{-1})	17271	17301	17301	17301	17301
ν_{01} (cm^{-1})	16978	16978	16949	16978	16978
ν_{02} (cm^{-1})	16393	16367	16340	16340	16340
ν_{03} (cm^{-1})	15361	15361	15385	15385	15361
ν_{04} (cm^{-1})	14245	14286	14327	14265	14327
I_{01}	137.72	22.36	1.72	4.88	8.07
I_{02}	1133.25	283.84	9.75	44.61	48.03
C_{Eu} (mol %)	100	0.97	1.25	0.15	1.51
I_{02}/C_{Eu}	11.33	298.33	7.80	297.40	30.23
I_{02}/I_{01}	8.23	13.19	5.67	14.23	5.95
Ω_2 ($\times 10^{-20}$ cm^2)	13.87	22.38	9.66	17.24	10.16
Ω_4 ($\times 10^{-20}$ cm^2)	0.33	0.52	0.43	0.57	0.54
τ (ms)	0.70	0.49	0.30	0.32	0.39
τ_{exp}^{-1} (s^{-1})	1429	2041	3333	3125	2564
A_{rad}^{0-4} (s^{-1})	436	768	362	604	374
A_{nrad}^{0-4} (s^{-1})	993	1273	2971	2521	2190
η_{lnt} (%)	30.51	37.61	10.86	19.33	14.60

[a] The energies of the $^5D_0 \rightarrow {}^7F_J$ transitions (ν_{0J}), the emission intensity of the $^5D_0 \rightarrow {}^7F_1$ transition (I_{01}) and the $^5D_0 \rightarrow {}^7F_2$ transition (I_{02}), the contents of the Eu^{3+} (C_{Eu}), the emission intensity of the $^5D_0 \rightarrow {}^7F_2$ transition divided by the contents of the Eu (I_{02}/C_{Eu}), the intensity ratios between the $^5D_0 \rightarrow {}^7F_2$ and $^5D_0 \rightarrow {}^7F_1$ transitions (I_{02}/I_{01}), experimental intensity parameters (Ω_λ), lifetimes (τ), radiative decay rates (A_{rad}), nonradiative decay rates (A_{nrad}), and the emission quantum efficiency (η) of the $^5D_0$ Eu^{3+} excited state were obtained at room temperature.

typical luminescence lines of Eu^{3+} ion at 578, 590, 611, 651, and 700 nm, corresponding to $^5D_0 \rightarrow {}^7F_J$ transitions ($J = 0$, 1, 2, 3, and 4, respectively). In comparison with the pure Eu(TTA)$_3$phen complex, the broadened emission lines and decreased number of Stark components suggest less ordered crystalline environments of Eu^{3+} ion in Eu(TTA)$_3$phen−SBA-15.[8b,25] Moreover, no emission from the triplet state of the phen or TTA ligands (no broad band emission in the blue and green spectral regions) is detected, indicating that the efficient energy transfer from the ligands to Eu^{3+} ion takes place. The difference in the excitation and emission spectra of Eu(TTA)$_3$phen and Eu(TTA)$_3$phen−SBA-15 shows that in the Eu(TTA)$_3$phen−SBA-15 mesoporous silica, the environment of ligands and the siloxo part of the structure affect the energy transfer.

In the case of SBA-15/Eu(TTA)$_3$ (Figure 10c) and SBA-15/Eu(TTA)$_3$phen (Figure 10d), the maximum absorptions of their excitation spectra shift to 341 and 350 nm, respectively, which are similar to the observed blue shift in Eu(TTA)$_3$phen−SBA-15. However, in the corresponding emission spectra of SBA-15/Eu(TTA)$_3$ ($\lambda_{ex} = 341$ nm) and SBA-15/Eu(TTA)$_3$phen ($\lambda_{ex} = 350$ nm), in addition to the typical emissions of Eu^{3+} ion, two weak peaks at 412 and 407 nm are observable, which are consistent with the emissions of the their host SBA-15 (see the short dashed line in Figure 10c, excited at 350 nm). The presence of the emissions of host SBA-15 suggests that in the above two samples the ligand-to-Eu^{3+} energy transfer is less efficient than in Eu(TTA)$_3$phen and Eu(TTA)$_3$phen-SBA-15. It is worth noting that the emission spectrum for Eu-phen-SBA-15 ($\lambda_{ex} = 279$ nm, Figure 10e) contains not only the emission of Eu^{3+} ion but also a broad emission band in the blue spectral region peaking around 452 nm. The broad emission band is mainly attributed to the $\pi^*-\pi$ relaxation of the free phen moiety,[8b,9] which is not able to completely transfer the absorbed energy to the central Eu^{3+} ion (see the short dashed line in Figure 10e, excited at 279 nm), while for Eu(TTA)$_3$phen-SBA-15, only the emission of Eu^{3+} ion is observed. Upon illumination of the Eu(TTA)$_3$phen-SBA-15 and Eu-phen-SBA-15 with a UV lamp ($\lambda = 365$ nm), the resulting Eu(TTA)$_3$phen-SBA-15 shows a pure red light and much stronger luminescence, which is in agreement with their emission spectra. As discussed above, compared with phen, TTA is a more efficient sensitizer for the luminescence of central Eu^{3+} ion and the intramolecular energy transfer from TTA ligand is more complete. The emission from the contribution of phen moiety in the blue region is too weak to be observed in Eu(TTA)$_3$phen-SBA-15. Therefore, the presence of β-diketone ligand TTA in the mesoporous matrix improved the luminescence properities of our prepared Eu(TTA)$_3$phen-SBA-15.

3.3.2. Luminescent Intensities. According to the literature reported previously,[8d] the luminescent intensities of the $^5D_0 \rightarrow {}^7F_2$ transition for all materials were compared. The contents of the Eu^{3+} ion in molar percentage [C_{Eu} (mol %)] in the Eu(TTA)$_3$phen complex, Eu(TTA)$_3$phen−SBA-15, SBA-15/Eu(TTA)$_3$, SBA-15/Eu(TTA)$_3$phen, and Eu−phen−SBA-15 and their relative luminescent intensities (integrated intensities) of the $^5D_0 \rightarrow {}^7F_2$ transition (I_{02}) are listed in Table 2. It can be clearly seen that the I_{02}/C_{Eu} (the intensity divided by the contents of the Eu^{3+} ion) in Eu(TTA)$_3$phen−SBA-15 is the highest in these samples. Compared with Eu(TTA)$_3$phen, when the complex is covalently bonded to mesoporous silica SBA-15, the I_{02}/C_{Eu} of Eu(TTA)$_3$phen−SBA-15 increases 25 times, which suggests that in the Eu(TTA)$_3$phen complex a quenching of the europium luminescence can be induced by the concentration effect and/or the electron−phonon couplings with the third vibrational overtone of the close-lying OH oscillator. This behavior shows that SBA-15 is an excellent host for the luminescent complex Eu(TTA)$_3$phen because the luminescence quenching of Eu^{3+} ion can be effectively decreased in this host. We found that SBA-15/Eu(TTA)$_3$phen exhibited relative a high I_{02}/C_{Eu} compared with Eu(TTA)$_3$phen−SBA-15. However, the I_{02} of SBA-15/Eu(TTA)$_3$phen is much lower than that of Eu(TTA)$_3$phen−SBA-15 because of the concentration limitation of Eu^{3+} ion in SBA-15/Eu(TTA)$_3$phen. For the SBA-15/Eu(TTA)$_3$ sample, the lowest I_{02}/C_{Eu} is probably related to the presence of water molecules coordinated to Eu^{3+} ion, which induces luminescence quenching of Eu^{3+} ion via OH vibrations.

In addition, since the $^5D_0 \rightarrow {}^7F_1$ transition does not depend on the chemical environments around the Eu^{3+} ion due to its magnetic dipole nature, it can be used as a reference to compare luminescent intensities of different Eu^{3+}-based materials. The relative luminescent intensities of the $^5D_0 \rightarrow {}^7F_1$ transition (I_{01}) and the $^5D_0 \rightarrow {}^7F_2$:$^5D_0 \rightarrow {}^7F_1$ intensity ratios (I_{02}/I_{01}) for all materials are also listed in Table 2. By comparison, it can be seen that the I_{02}/I_{01} values for Eu(TTA)$_3$phen−SBA-15 and

SBA-15/Eu(TTA)$_3$phen are higher than for the other three materials, which is in agreement with the I_{02}/C_{Eu} results.

3.3.3. Luminescence Decay Times. The luminescence decay profiles relative to the five materials could be fitted with single exponentials, from which the room temperature (RT) fluorescence lifetimes were calculated to confirm that all the Eu^{3+} ions detect the same average environment. The resulting lifetimes (shown in Table 2) are on the same order of magnitude for all samples. However, it appears that the lifetimes in hybrid materials are lower than that in the Eu(TTA)$_3$phen complex. This can be attributed to a possible quenching by OH or silanol groups in hybrid materials. Note that the fluorescence lifetime of Eu^{3+} ion in SBA-15/Eu(TTA)$_3$ (0.30 ms) is much shorter than that in Eu(TTA)$_3$phen−SBA-15 (0.49 ms). This, together with much lower I_{02}/C_{Eu} for the Eu^{3+} ion in SBA-15/Eu(TTA)$_3$, can be ascribed to a quenching effect by the OH group (from the coordinated H_2O) in SBA-15/Eu(TTA)$_3$,[3,5a] while in Eu(TTA)$_3$phen−SBA-15, the replacement of the water molecule in the first coordination sphere by the second ligand phen efficiently shields Eu^{3+} ion from the coordinated H_2O and better sensitizes Eu^{3+} ion luminescence, which results in stronger emission and a longer luminescence lifetime. It is evident from the above results that in Eu(TTA)$_3$phen−SBA-15, Eu^{3+} ion is mostly present as Eu(TTA)$_3$phen which is covalently bonded to the network, instead of as the Eu(TTA)$_3$·2H_2O complex.

3.3.4. Emission Quantum Efficiencies (η). On the basis of the emission spectra and lifetimes of the $^5D_0$ emitting level, the emission quantum efficiency (η) of the $^5D_0$ europium ion excited state can be determined. First, the emission intensity, I, taken as integrated intensity S of the $^5D_0 \rightarrow {}^7F_{0-4}$ emission curves, can be defined as

$$I_{i-j} = \hbar\omega_{i-j}A_{i-j}N_i \approx S_{i-j} \tag{1}$$

where i and j are the initial ($^5D_0$) and final levels ($^7F_{0-4}$), respectively, $\hbar\omega_{i-j}$ is the transition energy, A_{i-j} is the Einstein's coefficient of spontaneous emission, and N_i is the population of the $^5D_0$ emitting level.[26] The branching ratio for the $^5D_0 \rightarrow {}^7F_5$ and $^5D_0 \rightarrow {}^7F_6$ transitions must be neglected as they are not detected experimentally. Therefore, we can ignore their influence in the depopulation of the $^5D_0$ excited state.[27] Since the magnetic dipole $^5D_0 \rightarrow {}^7F_1$ transition is relatively insensitive to the chemical environments around the Eu^{3+} ion, and thus can be considered as a reference for the whole spectrum, the experimental coefficients of spontaneous emission, A_{0J}, were calculated according to the relation[28]

$$A_{0J} = A_{01}(I_{0J}/I_{01})(\nu_{01}/\nu_{0J}) \tag{2}$$

where ν_{01} and ν_{0J} are the energy baricenters of the $^5D_0 \rightarrow {}^7F_1$ and $^5D_0 \rightarrow {}^7F_J$ transitions, respectively.[28] A_{01} is the Einstein's coefficient of spontaneous emission between the $^5D_0$ and $^7F_1$ levels. Since in vacuo, $(A_{0-1})_{vac} = 14.65\ s^{-1}$, when an average index of refraction n equal to 1.506 was considered, the value of $A_{0-1} = n^3(A_{0-1})_{vac} \approx 50\ s^{-1}$.[29] Lifetime, radiative (A_{rad}), and nonradiative (A_{nrad}) transition rates are related through the following equation[27]

$$A_{tot} = \frac{1}{\tau} = A_{rad} + A_{nrad} \tag{3}$$

where A_{rad} can be obtained by summing over the radiative rates A_{0J} for each $^5D_0 \rightarrow {}^7F_J$ transition

$$A_{rad} = A_{01}\frac{\nu_{01}}{I_{01}}\sum_{J=0}^{4}\frac{I_{0J}}{\nu_{0J}} = \sum_J A_{0J} \tag{4}$$

Assuming that only nonradiative and radiative processes are essentially involved in the depopulation of the $^5D_0$ state, η can be expressed as

$$\eta = \frac{A_{rad}}{A_{rad} + A_{nrad}} \tag{5}$$

When eqs 1−5 are applied, the parameters A_{rad} and A_{nrad} and the quantum efficiency values, η, for the $^5D_0$ Eu^{3+} ion excited state in the five samples can be obtained, as shown in Table 2. As one can see, the quantum efficiencies of Eu(TTA)$_3$phen (η = 30.51) and Eu(TTA)$_3$phen−SBA-15 (η = 37.61) are higher than those of the other three materials. In addition, the quantum efficiency of Eu(TTA)$_3$phen−SBA-15 is higher than that of Eu(TTA)$_3$phen. This clearly demonstrates the modifications in the Eu^{3+} ion local environment as Eu(TTA)$_3$phen is covalently bonded to SBA-15 mesoporous material. The lowest quantum efficiency (η = 10.86) in SBA-15/Eu(TTA)$_3$ reflects the high nonradiative rate ($A_{nrad} = 2971\ s^{-1}$) arising from the luminescence quenching of the $^5D_0$ emitting level by OH oscillators of the water molecules in the first coordination sphere, which proves Eu^{3+} ion is covalently bonded to the silica network in Eu(TTA)$_3$phen−SBA-15. The low quantum efficiency (η = 19.33) for SBA-15/Eu(TTA)$_3$phen suggests that nonradiative processes are operative possibly due to vibronic coupling with the vibration of OH or silanol, which considerably quench the luminescence of Eu^{3+} ion, while in Eu(TTA)$_3$phen−SBA-15, we observed the higher emission quantum efficiency of the $^5D_0$ Eu^{3+} ion excited state due to the lower nonradiative transition rate. This can be ascribed to the substitution of the silanol with covalently bonded phen groups in the pore channel of mesoporous SBA-15, which results in the decrease in the level of nonradiative multiphonon relaxation by coupling to −OH vibrations and nonradiative transition rate. The results described above further confirm that Eu(TTA)$_3$phen is successfully covalently bonded to the SBA-15 network and organometallic complexes covalently bonding to the silica backbone might provide an effective approach to synthesizing lanthanide complex-functionalized mesoporous silica. Furthermore, Eu−phen−SBA-15 (η = 14.60) exhibits much lower emission quantum efficiency than Eu(TTA)$_3$phen−SBA-15, which shows that the introduced TTA ligand in Eu(TTA)$_3$phen−SBA-15 can efficiently activate the luminescence of Eu^{3+} ion.

3.3.5. Judd−Ofelt Parameters. The experimental intensity parameters (Ω_λ, λ = 2 and 4) were determined from the emission spectra for Eu^{3+} ion in Figure 9 based on the $^5D_0 \rightarrow {}^7F_2$ and $^5D_0 \rightarrow {}^7F_4$ transitions and the $^5D_0 \rightarrow {}^7F_1$ magnetic dipole-allowed transition as the reference, and they are estimated according to the equation[26,28,30]

$$A = \frac{4e^2\omega^3}{3\hbar c^3}\frac{1}{2J+1}\chi\sum_\lambda \Omega_\lambda \langle {}^5D_0||U^{(\lambda)}||{}^7F_J\rangle^2 \tag{6}$$

where $A_{0\lambda}$ is the coefficient of spontaneous emission, e is the electronic charge, ω is the angular frequency of the transition, $\hbar$ is Planck's constant over 2π, c is the velocity of light, χ is the Lorentz local field correction that is given by $n(n^2+2)^2/9$ with the refraction index n = 1.5,[26] and $\langle {}^5D_0||U^{(\lambda)}||{}^7F_J\rangle^2$ values are the square reduced matrix elements whose values are 0.0032 and 0.0023 for J = 2 and 4,[31] respectively. The Ω_6 parameter

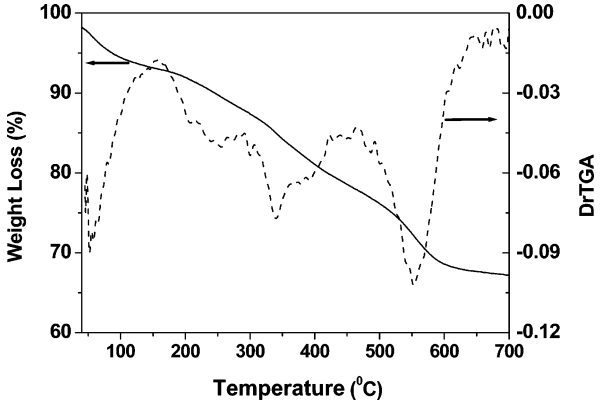

Figure 11. TGA (—) and DrTGA (– – –) curves of Eu(TTA)$_3$phen−SBA-15.

was not determined since the $^5D_0 \rightarrow {}^7F_6$ transition could not be experimentally detected.

The Ω_2 and Ω_4 intensity parameters for the five hybrid materials are presented in Table 2. A point to be noted in these results is the relatively high value of the Ω_2 intensity parameter for Eu(TTA)$_3$phen−SBA-15. This might be interpreted as being a consequence of the hypersensitive behavior of the $^5D_0 \rightarrow {}^7F_2$ transition. The dynamic coupling mechanism is, therefore, dominant, indicating that the Eu^{3+} ion is in a highly polarizable chemical environment and suggesting an improvement of the luminescence in Eu(TTA)$_3$phen−SBA-15 when compared with that exhibited by the Eu(TTA)$_3$phen complex.[26,30a,32]

3.4. Thermogravimetric Analysis. The thermal stability of Eu(TTA)$_3$phen−SBA-15 was demonstrated by TGA measurement. Figure 11 shows the thermogravimetric weight loss curve (TGA) and derivative weight loss (DrTGA) curve of Eu(TTA)$_3$phen−SBA-15. Three main weight loss peaks can be seen from the DrTGA curve. The first weight loss (approximately 5%) peak observed at ∼62 °C is due to physically adsorbed water. This is followed by a weight loss (approximately 12%) peak at ∼340 °C due to the thermal decomposition of incompletely removed surfactant.[13c] The third weight loss (approximately 14%) peak at 557 °C can be attributed to the decomposition of the organic lanthanide complex. In addition, the weight loss peak of the pure Eu(TTA)$_3$phen complex was reported to be at ∼340 °C,[11] suggesting that the thermal stability of the lanthanide complex was enhanced as it was covalently introduced into the mesoporous matrix.

4. Conclusions

Luminescent mesoporous silica SBA-15 covalently bonded with ternary lanthanide complex Eu(TTA)$_3$phen was prepared via a co-condensation method and a ligand exchange reaction. Our prepared Eu(TTA)$_3$phen−SBA-15 exhibits a strong, nearly monochromatic emission of Eu^{3+} ions, and good thermal stability. The differences in the profiles of the $^5D_0 \rightarrow {}^7F_{0-4}$ transitions, in luminescence intensity I_{02}/C_{Eu} of the $^5D_0 \rightarrow {}^7F_2$ transition, and in the $^5D_0$ lifetimes among all the synthesized materials confirm ternary complex Eu(TTA)$_3$phen is covalently bonded to the network of final Eu(TTA)$_3$phen−SBA-15 and demonstrate that the method of covalently bonding organometallic complexes to the silica backbone is more effective than the conventional method of doping mesoporous silica with organometallic complexes. Moreover, compared with SBA-15 covalently bonded with the binary europium complex, the introduction of β-diketone ligand TTA into the mesoporous matrix results in more efficient narrow bandwidth emission of red light. These conclusions were quantitatively stressed by calculating emission quantum efficiency η and experimental intensity parameters Ω_2 and Ω_4. The interactions between the organic complex and the silica matrix however need to be fundamentally investigated further.

Acknowledgment. This work is financially supported by the National Natural Science Foundation of China (Grant 20372060), the Key National Natural Science Foundation of China (Grant 20131010), the Important National Natural Science Foundation of China (Grant 20490210), the "863" National Foundation for High Technology Development and Programming (Grant 2002AA302105, 2002AA324080), and the Foreign Communion & Cooperation of the National Natural Science Foundation of China (Grant 20340420326).

References and Notes

(1) Sato, S.; Wada, M. *Bull. Chem. Soc. Jpn*. **1970**, *43*, 1955−1962.
(2) Serra, O. A.; Rosa, I. L. V.; Medeiros, C. L.; Zaniquell, M. E. D. *J. Lumin*. **1994**, *60−61*, 112−114.
(3) Binnemans, K.; Lenaerts, P.; Driesen, K.; Görller-Walrand, C. *J. Mater. Chem*. **2004**, *14*, 191−195.
(4) (a) Liu, F. Y.; Fu, L. S.; Wang, J.; Liu, Z.; Li, H. R.; Zhang, H. J. *Thin Solid Films* **2002**, *419*, 178−182. (b) Dong, D. W.; Jiang, S. C.; Men, Y. F.; Ji, X. L.; Jiang, B. Z. *Adv. Mater*. **2000**, *12*, 646−649.
(5) (a) Li, H. R.; Lin, J.; Zhang, H. J.; Fu, L. S.; Meng, Q. G.; Wang, S. B. *Chem. Mater*. **2002**, *14*, 3651−3655. (b) Franville, A. C.; Zambon, D.; Mahiou, R. *Chem. Mater*. **2000**, *12*, 428−435. (c) Embert, F.; Mehdi, A.; Reyé, C.; Corriu, R. J. P. *Chem. Mater*. **2001**, *13*, 4542−4549.
(6) (a) Kresge, C. T.; Leonowicz, M. E.; Roth, W. J.; Vartuli, J. C.; Beck, J. S. *Nature* **1992**, *359*, 710−712. (b) Beck, J. S.; Vartuli, J. C.; Roth, W. J.; Leonowicz, M. E.; Kresge, C. T.; Schmitt, K. D.; Chu, C. T.-W.; Olson, D. H.; Sheppard, E. W.; McCullen, S. B.; Higgins, J. B.; Schlenker, J. L. *J. Am. Chem. Soc*. **1992**, *114*, 10834−10843.
(7) (a) De Vos, D. E.; Dams, M.; Sels, B. F.; Jacobs, P. A. *Chem. Rev*. **2002**, *102*, 3615−3640. (b) Davis, M. E. *Nature* **2002**, *417*, 813−821. (c) Stein, A. *Adv. Mater*. **2003**, *15*, 763−775. (d) Scott, B. J.; Wirnsberger, G.; Stucky, G. D. *Chem. Mater*. **2001**, *13*, 3140−3150.
(8) (a) Xu, Q. H.; Li, L. S.; Liu, X. S.; Xu, R. R. *Chem. Mater*. **2002**, *14*, 549−555. (b) Bartl, M. H.; Scott, B. J.; Huang, H. C.; Wirnsberger, G.; Popitsch, A.; Chmelka, B. F.; Stucky, G. D. *Chem. Commun*. **2002**, 2474−2475. (c) Yao, Y. F.; Zhang, M. S.; Shi, J. X.; Gong, M. L.; Zhang, H. J.; Yang, Y. S. *J. Rare Earths* **2000**, *18*, 186−189. (d) Xu, Q. H.; Dong, W. J.; Li, H. W.; Li, L. S.; Feng, S. H.; Xu, R. R. *Solid State Sci.* **2003**, *5*, 777−782. (e) Meng, Q. G.; Boutinaud, P.; Franville, A.-C.; Zhang, H. J.; Mahiou, R. *Microporous Mesoporous Mater*. **2003**, *65*, 127−136.
(9) Li, H. R.; Lin, J.; Fu, L. S.; Guo, J. F.; Meng, Q. G.; Liu, F. Y.; Zhang, H. J. *Microporous Mesoporous Mater*. **2002**, *55*, 103−107.
(10) Frey, S. T.; Gong, M. L.; Horrocks, W. DeW., Jr. *Inorg. Chem*. **1994**, *33*, 3229−3234.
(11) Li, H. H.; Inoue, S.; Machida, K.; Adachi, G. *Chem. Mater*. **1999**, *11*, 3171−3176.
(12) (a) Zhao, D. Y.; Huo, Q. S.; Feng, J. L.; Chmelka, B. F.; Stucky, G. D. *J. Am. Chem. Soc*. **1998**, *120*, 6024−6036. (b) Zhao, D. Y.; Feng, J. L.; Huo, Q. S.; Melosh, N.; Fredrickson, G. H.; Chmelka, B. F.; Stucky, G. D. *Science*, **1998**, *279*, 548−552.
(13) (a) Corriu, R. J. P.; Mehdi, A.; Reyé, C.; Thieuleux, C.; Frenkel, A.; Gibaud, A. *New J. Chem.* **2004**, *28*, 156−160. (b) Corriu, R. J. P.; Mehdi, A.; Reyé, C.; Thieuleux, C. *Chem. Mater*. **2004**, *16*, 159−166. (c) Hu, Q. Y.; Hampsey, J. E.; Jiang, N.; Li, C. J.; Lu, Y. F. *Chem. Mater*. **2005**, *17*, 1561−1569.
(14) Lecomte, J.-P.; Mesmaeker, A. K.-D.; Demeunynck, M.; Lhomme, J. J. *Chem. Soc., Faraday Trans*. **1993**, *89*, 3261−3269.
(15) Matthews, L. R.; Knobbe, E. T. *Chem. Mater*. **1993**, *5*, 1697−1700.
(16) Melby, L. R.; Rose, N. J.; Abramson, E.; Caris, J. C. *J. Am. Chem. Soc.* **1964**, *86*, 5117−5125.
(17) (a) Lim, M. H.; Stein, A. *Chem. Mater*. **1999**, *11*, 3285−3295. (b) Huq, R.; Mercier, L. *Chem. Mater*. **2001**, *13*, 4512−4519. (c) Mercier, L.; Pinnavaia, T. J. *Chem. Mater*. **2000**, *12*, 188−196.
(18) Everett, D. H. *Pure Appl. Chem*. **1972**, *31*, 577−638.
(19) Wang, Y. Q.; Zibrowius, B.; Yang, C. M.; Spliethoff, B.; Schüth, F. *Chem. Commun*. **2004**, 46−47.
(20) (a) Okamoto, Y.; Ueba, Y.; Dzhanibekov, N. F.; Banks, E. *Macromolecules* **1981**, *14*, 17−22. (b) Kawa, M.; Fréchet, J. M. J. *Chem. Mater*. **1998**, *10*, 286−296. (c) Bekiari, V.; Lianos, P. *Adv. Mater*. **1998**, *10*, 1455−1458. (d) Sabbatini, N.; Mecati, A.; Guardigli, M.; Balzani, V.; Lehn, J. M.; Zeissel, R.; Ungaro, R. *J. Lumin*. **1991**, *48−49*, 463−468. (e)

Sabbatini, N.; Mecati, A.; Guardigli, M.; Balazani, V.; Lehn, J. M. *Coord. Chem. Rev.* **1993**, *93*, 201−228.

(21) (a) Förster, T. *Z. Naturforsch.*, **1949**, *A4*, 321. (b) Berlman, I. B. *Energy Transfer Parameters of Aromatic Compounds*; Academic Press: New York, 1973.

(22) (a) Crosby, G. A.; Whan, R. E.; Alire, R. M. *J. Chem. Phys*. **1961**, *34*, 743−748. (b) Filipescu, N.; Sager, W. F.; Serafin, F. A. *J. Phys. Chem*. **1964**, *68*, 3324−3346. (c) Sager, W. F.; Filipescu, N.; Serafin, F. A. *J. Phys. Chem*. **1965**, *69*, 1092−1100.

(23) Brito, H. F.; Liu, G. K. *J. Chem. Phys*. **2000**, *112*, 4334−4341.

(24) Bünzli, J. G.; Moret, E.; Foiret, V.; Schenk, K. J.; Wang, M.; Jin, L. *J. Alloys Compd*. **1994**, *207/208*, 107−111.

(25) (a) Polizzi, S.; Battagliarin, M.; Bettinelli, M.; Speghini, A.; Fagherazzi, G. *J. Mater. Chem.* **2002**, *12*, 742−747. (b) Boyer, J. C.; Vetrone, F.; Capobianco, J. A.; Speghini, A.; Bettinelli, M. *J. Phys. Chem. B* **2004**, *108*, 20137−20143.

(26) (a) Malta, O. L.; Couto dos Santos, M. A.; Thompson, L. C.; Ito, N. K. *J. Lumin.* **1996**, *69*, 77−84. (b) Malta, O. L.; Brito, H. F.; Menezes, J. F. S.; Gonçalves e Silva, F. R.; Alves, S., Jr.; Farias, F. S., Jr.; Andrade, A. V. M. *J. Lumin.* **1997**, *75*, 255−268.

(27) (a) Soares-Santos, P. C. R.; Nogueira, H. I. S.; Félix, V.; Drew, M. G. B.; Sá Ferreira, R. A.; Carlos, L. D.; Trindade T. *Chem. Mater*. **2003**, *15*, 100−108. (b) Sá Ferreira, R. A.; Carlos, L. D.; Gonçalves, R. R.; Ribeiro, S. J. L.; de Zea Bermudez, V. *Chem. Mater.* **2001**, *13*, 2991−2998. (c) Carlos, L. D.; Messaddeq, Y.; Brito, H. F.; Sá Ferreira, R. A.; de Zea Bermudez, V.; Ribeiro, S. J. L. *Adv. Mater.* **2000**, *12*, 594−598.

(28) Teotonio, E. E. S.; Espínola, J. G. P.; Brito, H. F.; Malta, O. L.; Oliveria, S. F.; de Foria, D. L. A.; Izumi, C. M. S. *Polyhedron* **2002**, *21*, 1837−1844.

(29) (a) Werts, M. H. V.; Jukes, R. T. F.; Verhoeven, J. W. *Phys. Chem. Chem. Phys*. **2002**, *4*, 1542−1548. (b) Hazenkamp, M. F.; Blasse, G. *Chem. Mater*. **1990**, *2*, 105−110. (c) Ribeiro, S. J. L.; Dahmouche, K.; Ribeiro, C. A.; Santilli, C. V.; Pulcinelli, S. H. J. *J. Sol-Gel Sci. Technol*. **1998**, *13*, 427−432.

(30) (a) de Sá, G. F.; Malta, O. L.; de Mello Donegá, C.; Simas, A. M.; Longo, R. L.; Santa-Cruz, P. A.; da Silva, E. F., Jr. *Coord. Chem. Rev.* **2000**, *196*, 165−195. (b) Boyer, J. C.; Vetrone, F.; Capobianco, J. A.; Speghini, A.; Bettinelli, M. *J. Phys. Chem. B* **2004**, *108*, 20137−20143. (c) Kodaira, C. A.; Claudia, A.; Brito, H. F.; Felinto, M. C. F. C. *J. Solid State Chem.* **2003**, *171*, 401−407.

(31) Carnall, W. T.; Crosswhite, H.; Crosswhite, H. M. *Energy level structure and transition probabilities of the trivalent lanthanides in* LaF_3; Argonne National Laboratory: Argonne, IL, 1978.

(32) Judd, B. R. *J. Chem. Phys*. **1979**, *70*, 4830−4833.